Video Article

Metal-silicate Partitioning at High Pressure and Temperature: Experimental Methods and a Protocol to Suppress Highly Siderophile Element Inclusions

Neil R. Bennett[1,2], James M. Brenan[1], Yingwei Fei[2]

[1]Department of Earth Science, University of Toronto

[2]Geophysical Laboratory, Carnegie Institution of Washington

Correspondence to: Neil R. Bennett at nbennett@carnegiescience.edu

URL: https://www.jove.com/video/52725
DOI: doi:10.3791/52725

Keywords: Chemistry, Issue 100, siderophile elements, geoengineering, primitive upper mantle (PUM), HSEs, terrestrial accretion

Date Published: 6/13/2015

Citation: Bennett, N.R., Brenan, J.M., Fei, Y. Metal-silicate Partitioning at High Pressure and Temperature: Experimental Methods and a Protocol to Suppress Highly Siderophile Element Inclusions. *J. Vis. Exp.* (100), e52725, doi:10.3791/52725 (2015).

Abstract

Estimates of the primitive upper mantle (PUM) composition reveal a depletion in many of the siderophile (iron-loving) elements, thought to result from their extraction to the core during terrestrial accretion. Experiments to investigate the partitioning of these elements between metal and silicate melts suggest that the PUM composition is best matched if metal-silicate equilibrium occurred at high pressures and temperatures, in a deep magma ocean environment. The behavior of the most highly siderophile elements (HSEs) during this process however, has remained enigmatic. Silicate run-products from HSE solubility experiments are commonly contaminated by dispersed metal inclusions that hinder the measurement of element concentrations in the melt. The resulting uncertainty over the true solubility and metal-silicate partitioning of these elements has made it difficult to predict their expected depletion in PUM. Recently, several studies have employed changes to the experimental design used for high pressure and temperature solubility experiments in order to suppress the formation of metal inclusions. The addition of Au (Re, Os, Ir, Ru experiments) or elemental Si (Pt experiments) to the sample acts to alter either the geometry or rate of sample reduction respectively, in order to avoid transient metal oversaturation of the silicate melt. This contribution outlines procedures for using the piston-cylinder and multi-anvil apparatus to conduct solubility and metal-silicate partitioning experiments respectively. A protocol is also described for the synthesis of uncontaminated run-products from HSE solubility experiments in which the oxygen fugacity is similar to that during terrestrial core-formation. Time-resolved LA-ICP-MS spectra are presented as evidence for the absence of metal-inclusions in run-products from earlier studies, and also confirm that the technique may be extended to investigate Ru. Examples are also given of how these data may be applied.

Video Link

The video component of this article can be found at https://www.jove.com/video/52725/

Introduction

Terrestrial accretion is thought to have occurred as a series of collisions between planetesimals with a chondritic bulk composition, terminating in a giant-impact phase thought responsible for moon formation[1,2]. Heating of the proto-earth by impacts and the decay of short-lived isotopes was sufficient to cause extensive melting and the formation of a magma ocean or ponds through which dense Fe-rich metallic melts could descend. Upon reaching the base of the magma ocean, metallic melts encounter a rheological boundary, stall, and undergo final metal-silicate equilibrium before eventually descending through the solid mantle to the growing core[2]. Further chemical communication between metal and silicate phases as metallic melt traverses the solid portion of the mantle is thought to be precluded due to the large size and rapid descent of metal diapirs[3]. This primary differentiation of the Earth into a metallic core and silicate mantle is revealed today by both geophysical and geochemical observations[4–6]. Interpreting these observations to yield plausible conditions for metal-silicate equilibrium at the base of a magma ocean, however, requires an appropriate database of experimental results.

The primitive upper mantle (PUM) is a hypothetical reservoir comprising the silicate residue of core formation and its composition therefore reflects the behaviour of trace elements during metal-silicate equilibrium. Trace elements are distributed between metal and silicate melts during core segregation on the basis of their geochemical affinity. The magnitude of an elements preference for the metal phase can be described by the metal-silicate partition coefficient $\left(D_i^{Met/Sil}\right)$:

$$D_i^{Met/Sil} = \frac{C_i^{Met}}{C_i^{Sil}} \quad (1)$$

Where C_i^{Met} and C_i^{Sil} denote the concentration of element *i* in metal and silicate melt respectively. Values of $D_i^{Met/Sil}$ >1 indicate siderophile (iron-loving) behaviour and those <1 lithophile (rock-loving) behavior. Estimates of the PUM composition show that siderophile elements are depleted relative to chondrites[7], typically considered as representative of Earth's bulk composition[6,8]. This depletion is due to sequestration of siderophile elements by the core, and for refractory elements its magnitude should directly reflect values of $D_i^{Met/Sil}$. Lab experiments therefore

seek to determine values of $D_i^{Met/Sil}$ over a range of pressure (*P*), temperature (*T*) and oxygen fugacity (fO_2) conditions that are relevant to metal segregation from the base of a magma ocean. The results of these experiments may then be used to delineate regions of *P-T-*fO_2 space that are compatible with the PUM abundance of multiple siderophile elements (*e.g.,*[9–11]).

The high pressures and temperatures relevant to a magma ocean scenario can be recreated in the laboratory using either a piston-cylinder or multi-anvil press. The piston-cylinder apparatus provides access to moderate pressure (~2 GPa) and high temperature (~2,573 K) conditions, but enables large sample volumes and a variety of capsule materials to be easily used. The rapid cooling rate also permits quenching of a range of silicate melt compositions to a glass, thus simplifying textural interpretation of the run-products. The multi-anvil apparatus typically employs smaller sample volumes but with suitable assembly designs can achieve pressures up to ~27 GPa and temperatures of ~3,000 K. The use of these methods has allowed partitioning data for many of the moderately and slightly siderophile elements to be gathered over a large range of *P-T* conditions. Predictions of the PUM composition based on these data suggest metal-silicate equilibrium occurred at average pressure and temperature conditions in excess of ~29 GPa and 3,000 K respectively, although the exact values are model dependent. In order to account for the PUM abundance of certain redox sensitive elements (*e.g.,* V, Cr) the fO_2 is also thought to evolve during accretion from ~4 to 2 log units below that imposed by co-existing iron and wüstite (FeO) at equivalent *P-T* conditions (the iron-wüstite buffer)[12].

Although the PUM abundance of many siderophile elements can be accounted for by metal-silicate equilibrium at the base of a deep magma ocean, it has proved difficult to assess if this situation also applies to the most highly siderophile elements (HSEs). The extreme affinity of the HSEs for iron-metal indicated by low pressure (*P* ~0.1 MPa) and temperature (*T* <1,673 K) experiments suggests the silicate earth should be strongly depleted in these elements. Estimates of the HSE content for PUM, however, indicate only a moderate depletion relative to chondrite (**Figure 1**). A commonly posited solution to the apparent HSE excess is that Earth experienced a late-accretion of chondritic material subsequent to core-formation[13]. This late-accreted material would have mixed with the PUM and elevated HSE concentrations but had a negligible effect on more abundant elements. Alternatively, it has been suggested that the extremely siderophile nature of HSEs indicated by low *P-T* experiments does not persist to the high *P-T* conditions present during core-formation[14,15]. In order to test these hypotheses, experiments must be carried out to determine the solubility and metal-silicate partitioning of HSEs at appropriate conditions. Contamination of the silicate portion of quenched run-products in many previous studies however, has complicated run-product analysis and obscured the true partition coefficients for HSEs between metal and silicate melts.

In partitioning experiments where the HSEs are present at concentration levels appropriate to nature, the extreme preference of these elements for Fe-metal prevents their measurement in the silicate melt. To circumvent this problem, solubility measurements are made in which the silicate melt is saturated in the HSE of interest and values of $D_i^{Met/Sil}$ are calculated using the formalism of Borisov *et al.*[16]. Quenched silicate run-products from HSE solubility experiments performed at reducing conditions, however, often display evidence for contamination by dispersed HSE±Fe inclusions[17]. Despite the near ubiquity of these inclusions in low fO_2 experiments containing Pt, Ir, Os, Re and Ru, (*e.g.,* [18–27]), there is notable variability between studies in their textural presentation; compare for example references [22] and [26]. Although it has been demonstrated that inclusions can form which are a stable phase at the run conditions of an experiment[28], this does not preclude the formation of inclusions as the sample is quenched. Uncertainty surrounding the origin of inclusions makes the treatment of analytical results difficult, and has led to ambiguity over the true solubility of HSEs in reduced silicate melts. Inclusion-free run-products are required to assess which studies have adopted an analytical approach that yields accurate dissolved HSE concentrations. Considerable progress in suppressing the formation of metal-inclusions at reducing conditions has now been demonstrated in experiments using a piston-cylinder apparatus, in which the sample design was amended from previous studies by adding either Au or Si to the starting materials[29–31]. The addition of Au or elemental Si to the starting materials alters the sample geometry or fO_2 evolution of the experiment respectively. These methods are intended to suppress metal inclusion formation by altering the timing of HSE in-diffusion versus sample reduction, and are discussed in Bennett *et al.*[31]. Unlike some previous attempts to cleanse the silicate melt of inclusions, such as mechanically assisted equilibration and the centrifuging piston-cylinder, the present protocol can be implemented without specialized apparatus and is suitable for high *P-T* experiments.

Described in detail here is a piston-cylinder based approach to determine the solubility of Re, Os, Ir, Ru, Pt and Au in silicate melt at high temperature (>1,873 K), 2 GPa and an fO_2 similar to that of the iron-wüstite buffer. Application of a similar experimental design may also prove successful in HSE experiments at other pressures, providing the required phase relations, wetting properties and kinetic relationships persist to the chosen conditions. Existing data however, are insufficient to predict whether our sample design will be successful at pressures corresponding to a deep magma ocean. Also outlined is a general approach used to determine moderately and slightly siderophile element (MSE and SSE respectively) partitioning using a multi-anvil device. Extension of the inclusion-free dataset for HSEs to high pressure is likely to employ similar multi-anvil methods. Together, these procedures provide a means to constrain both the conditions of core-segregation and the stages of terrestrial accretion.

Protocol

1) Preparation of Starting Material

1. Synthetic Basalt
   Note: A basaltic composition is used as the silicate starting material as more depolymerized compositions, although more relevant to a magma ocean scenario, are difficult or impossible to quench to a glass in piston-cylinder and multi-anvil experiments.
   1. Weigh the desired amounts of component oxide or carbonate (Ca and Na) powders, with the exception of Fe, and add to an agate mortar (see example in **Table 1**). An Fe-free mixture weighing ~4 g should provide sufficient starting material for an extensive suite of experiments.
   2. Add ethanol to the agate mortar until the powders are submerged then grind for at least 2 hr using an agate pestle to homogenize both the composition and grain size of the mixture.
      Note: Homogeneity of ground starting compositions can be checked by examining a pressed pellet of the powdered mixture with a scanning electron microscope equipped for compositional analysis by energy dispersive x-ray spectroscopy.

3. Once thoroughly homogenized, place the mortar under a 250 W heat lamp, at a distance of ~20 cm. After the powdered mixture is dry, which may take 20-60 min, transfer it to either an alumina or mullite (an alumino-silicate) crucible.
4. To decarbonate the mixture, place the crucible with the powdered mixture into a box furnace at RT and ramp to 1,273 K over the course of 3-5 hr. Leave the mixture in the furnace at 1,273 K O/N.
5. Remove the decarbonated mixture from the box furnace and allow it to cool to RT. Once cool, weigh and add iron to the mixture as either FeO or Fe_2O_3 powder (see **Table 1**). Varying the ratio of FeO to Fe_2O_3 while keeping the total Fe content the same allows the final fO_2 of the sample to be changed. To access more reducing conditions, and in all experiments to investigate Pt, also add ~0.5-2.0 wt% Si to the mixture. Once Fe (±Si) has been added, re-homogenize the mixture by again grinding under ethanol with an agate mortar and pestle.
6. Dry the homogenized mixture under a heat lamp and then transfer it to a shell vial. Store in a desiccator until ready to load the sample capsule.

2. Metallic Phase: Re, Os, Ir, Ru Experiments
   1. For experiments intended to investigate Re, Os, Ir or Ru, prepare a 3:1 by weight (6:1 for Ru, to account for the difference in atomic mass) mixture of Au and the HSE of interest, using high purity metallic powders. A mixture weighing ~500 mg should provide sufficient starting material for an extensive suite of experiments.
   2. Transfer the mixture into a graphite crucible and cover with a graphite lid. Then place the covered crucible into a box furnace at a temperature of 1,473 K for ~5 min. Once removed from the furnace, leave the crucible lid in place until the assembly has cooled to RT.
      CAUTION: Heating of osmium in air may result in formation of the toxic compound osmium tetroxide. Osmium metal is also a known skin irritant, see MSDS for CAS# 7440-04-2.
      Note: This process melts the Au (melting point ~1,337 K) but not the accompanying HSE, resulting in formation of a metallic bead where the HSE of interest is surrounded by a rind of Au.
   3. Remove the metallic bead from the graphite crucible and use a razor blade to divide it into smaller pieces which measure ~1 mm in their longest dimension. Once cut, place the beads into a shell vial and store in a desiccator.

3. Metallic Phase: Pt Experiments
   Note: Experiments to investigate Pt cannot be performed using the Au-coated bead technique due to the complete miscibility of Pt and Au at high temperature (>2,042 K at 0.1 MPa[32]). This precludes a sample geometry whereby Pt is physically separated from the silicate melt during an experiment by a rind of Au.
   1. Thoroughly mix metallic powders of Pt and Ir in a 1:1 ratio by weight to make a total of ~500 mg of mixture. Next, add ~20 mg of metallic Fe powder so that Fe comprises ~4 weight percent of the total mixture.
   2. Tape a clean drill blank (alternatively, the shank of a drill may be used in place of a drill blank) to the edge of a workbench so that ~3 mm protrudes from the tabletop. Position a silica glass tube, with an internal diameter of ~2-3 mm and external diameter of ~4-6 mm, onto the protruding end of the drill blank.
   3. Place the PtIrFe mixture into the glass tube and insert another drill blank above it. Both drill blanks should have a diameter not more than 0.1 mm smaller than the inner diameter of the silica glass tube. Cold-press the metallic mixture by pushing the drill blanks together by hand (**Figure 2**).
      CAUTION: Use of excessive force during the cold-pressing step can cause the silica glass to shatter).
   4. Put the cold-pressed powders, still inside the silica glass tube, into an alumina crucible and suspend in the cool portion of a gas-mixing vertical tube furnace. Increase the furnace temperature to 1,673 K and using CO-CO_2 gas mixtures, set the furnace fO_2 to a value close to the iron-wüstite buffer.
      Note: At ambient pressure and 1,673 K, the iron-wüstite buffer corresponds to a fO_2 of 1.93×10^{-10} Pa[33]. The relationship between CO-CO_2 mixing ratio, temperature and fO_2 can be found in reference [34]. For the iron-wüstite buffer at 1,673 K use a gas mixture comprising 22.25 vol% CO_2 and 77.75 vol% CO.
      1. Once the desired temperature and fO_2 are reached, lower the alumina crucible so that it resides in the furnace hot spot and leave O/N for the pressed powders to anneal.
   5. Remove the crucible and pressed powders from the gas-mixing furnace and allow them to cool. If the silica glass tube is still intact, use a drill blank to push the annealed powder out of the tube. Using wire cutters, break the annealed powder into pieces small enough to fit within the sample capsule chosen for the experiment.
   6. Transfer the metallic pieces to a shell vial and store in a desiccator until required.

4. Metallic Phase: Multi-anvil Experiments
   1. For experiments to determine the partitioning of moderately and slightly siderophile elements, mix the synthetic basalt powder with Fe-metal powder in equal proportions.
      Note: Some portion of the Fe may be added as a Fe-Si alloy, typically so that Si comprises <8 wt% of the metallic fraction. This will ensure the experimental fO_2 remains low.
   2. Add the chosen trace elements as metal-oxide powders to the basalt plus metal mixture. Homogenize the starting material by grinding under ethanol with an agate mortar and pestle. The exact amount of trace elements added will depend upon the element being investigated, however, nominal concentrations of several thousand ppm to 2 wt% are typical[10,35].
   3. Once homogenized, dry the powdered starting material under a heat lamp, transfer it to a shell vial then store in a desiccator until needed.

2. Preparation of Assembly Components

1. Piston Cylinder
   Note: The piston cylinder assembly consists of a graphite capsule that is supported in the hot spot of a graphite resistance heater using crushable magnesia pieces. An alumina sheathed thermocouple is positioned axially through the upper portion of the assembly to monitor temperature at the top of the sample. The furnace is then surrounded by $BaCO_3$ cells which act as both a pressure medium and thermal

insulator[36]. The assembly dimensions are provided in **Figure 3A**. A list of example materials used for the experiments and their sources are provided in **Table 2**.

1. Machine the graphite capsules, graphite end plug and magnesia support pieces to the required dimensions with a center lathe, using high purity graphite and magnesia rods or tubes respectively as starting materials (**Figure 3A**).
   Note: For experiments to investigate Re, Os and Ir, HSE-Fe alloys may be substituted for graphite as the capsule material[29,30].
2. Sonicate the graphite capsules in ethanol for ~1 min at RT, then dry under a heat lamp in the same manner as directed for powdered starting materials. Once dry, transfer the capsules to a shell vial and store in a desiccator or drying oven until required.
3. Place the magnesia support pieces in either an alumina or mullite crucible and anneal at 1,573 K in a box furnace for at least 8 hr. After annealing, allow the pieces to cool then store in a drying oven maintained at ~393 K.
4. To make the barium carbonate cells, first mix $BaCO_3$ powder and used copy toner in 99:1 proportions by weight. A minimum of 7.4 grams of mixture is required for one experiment. Coat the interior portion of an appropriately sized steel die (see **Figure 3A** for dimensions of the $BaCO_3$ sleeves) with either a graphite-based dry lubricant or PTFE-based mold release agent (**Table 2**).
5. Cold-press 3.7 g of the mixture to ~250 MPa using the steel die and a hydraulic press. Leave the mixture at pressure for 1 min before decompression. This will produce a sleeve with a height of 17 mm. Two sleeves are required for each assembly.
   Note: The 2-cell arrangement described above and used in some previous studies[29–31] may be substituted for a single $BaCO_3$ cell providing a suitably sized die is available.
6. Once removed from the die, drive-off the copy toner by heating the sleeves from RT to 923 K over the course of several hours in a box furnace, then holding at this temperature for ~30 min. Note the change in color from black to orange once the copy toner has been removed. Store the annealed sleeves in a drying oven maintained at ~393 K.

2. Multi-anvil
   Note: The multi-anvil assembly comprises a sample capsule that is positioned in the hot spot of a cylindrical graphite resistance heater using crushable MgO or Al_2O_3 filler pieces. The heater is surrounded by either a sintered or castable ceramic octahedron that acts as both a pressure medium and thermal insulator. The thermocouple may be positioned either axially or transversely depending upon the assembly design. There are numerous sizes and designs of assembly used for multi-anvil experiments, depending upon the desired objective and *P-T* conditions. **Figure 4** displays an assembly design previously used to perform metal-silicate partitioning experiments at 3.6 and 7.7 GPa[35].
   1. Prepare graphite capsules and crushable magnesia or zirconia sleeves from high purity tubes in the same manner as indicated for piston cylinder experiments. The required dimensions are provided in **Figure 4A**.
   2. Make the alumina plug from a length of hard-fired alumina rod. Use a diamond file to score the rod where it is to be broken, then snap the rod to the required length by hand (see **Figure 4A** for dimensions). Use the file to remove any burrs that result from breaking the rod. Clean the plug by sonicating it in ethanol at RT.
   3. Prepare octahedra with an 18 mm octahedral edge length (OEL) using an MgO-based castable 2-part ceramic (see **Table 2**) and appropriately sized mold. The mold comprises a jig which holds 8 truncated cubes, separated by sheets with a thickness equal to that desired for the pre-formed gaskets[37].
      1. For octahedra with an 18 mm OEL, use cubes with an 11 mm truncated edge length (TEL) and sheets that are 3 mm thick. Use either aluminum or PVC for the cube and sheet materials. Assemble the mold, lubricating all parts that will contact the castable ceramic with silicone grease. Leave one cube unassembled to provide an entry point for the ceramic mixture.
      2. Combine the powder ceramic and liquid activator in a 100:30 ratio by weight and mix thoroughly. Pour the mixture into the mold, ensuring there are no trapped pockets of air. Insert the remaining cube and allow the mixture to set for at least 2 hr. Each octahedron requires ~15 g of ceramic mixture.
   4. Once set, remove the octahedron from the mold, dehydrate for ~1 day in a drying oven at 393 K then anneal at 1,273-1,373 K in a box furnace for ~2 hr.
   5. Allow the octahedron to cool to RT in air, then drill a 7.3 mm diameter hole as indicated in **Figure 4B** to accommodate the insulating sleeve, graphite heater and remaining sample components.
   6. Store in a drying oven at ~393 K until ready to assemble the experiment.

3. Assembly of the Components

1. Assembly of the Piston-cylinder Experiment
   1. Load the graphite sample capsule by first inserting the HSE-bearing metal then adding synthetic basalt powder until the capsule is filled. Use of a gravitationally stable arrangement minimizes the chance for overturn during the experiment and is intended to prevent dispersion of the metallic phase through mechanical action.
   2. Place a small amount (typically <50 mg) of dry MgO powder at the base of the cavity designed to hold the sample capsule. This flattens the tapered surface created when drilling the hole and in turn reduces shear forces during sample compression that may crack the capsule.
   3. Assemble all the previously made components as shown in **Figure 3B**.
   4. Wrap a piece of 30 µm thick lead foil around the assembly, folding a small (~1.5 mm) portion of foil over the exposed end of the lower $BaCO_3$ sleeve. Insert the assembly into a 12.7 mm bore tungsten carbide pressure vessel, along with a base plug (above) and steel end-piece (below) as shown in **Figure 3A**.
      Note: The end-loaded piston-cylinder apparatus has two hydraulic rams. A bridge straddling the lower ram allows a tungsten carbide piston to apply pressure to the bottom of the sample. The upper ram fixes the location of the upper sample surface and applies an end-load to the pressure vessel that gives additional support to the tungsten carbide core[38]. **Figure 3C** shows a piston cylinder apparatus at the University of Toronto with the bridge in place. A friction-correction of -9% is applied to account for the difference between the nominal sample pressure and that experienced by the sample[39].
   5. Position the bridge, pressure vessel and base-plate between the hydraulic rams. Next make a C-type thermocouple using 4-hole hard-fired alumina tube with an outer diameter of 1.6 mm. The alumina tube should be cut sufficiently long to allow ~1-2 mm of the tube to protrude from the upper surface of the top-plate.

6. Feed both wire compositions (see **Table 2**) through adjacent holes in the tube, turn the ends through 180 degrees and secure them in the opposing holes so that the wires cross. Insert the thermocouple through the top plate and into the assembly, so that the junction is directly above the sample. Insulate the remainder of the thermocouple wires using flexible Teflon tubes, leaving a 10-20 mm portion exposed at the end.
7. Place any required metal spacers in place between the top plate and the upper ram. During assembly, position Mylar sheets both above the pressure vessel and between the top of the assembly and the upper ram. These sheets electrically isolate the sample heating circuit from the rest of the apparatus.

2. Assembly of the Multi-anvil Experiment
    1. Make a C-type thermocouple using 4-hole hard-fired alumina tube by feeding both wires through adjacent holes in the tube, turning the ends through 180° and securing them in the opposing holes. Insulate the remainder of the wires with a short length (~20 mm) of alumina tube and then Teflon insulating material, leaving a 10-20 mm portion of exposed wire at the end.
    2. Insert the zirconia sleeve and graphite heater into the octahedron, then cut grooves as indicated in **Figure 4B**. Insert the thermocouple into the top of the octahedron and position the alumina covered arms into the grooves. Use zirconia cement (see **Table 2**) to fill the void space surrounding the thermocouple and allow to dry.
    3. In order to isolate the thermocouple join from the graphite capsule, add MgO powder from the base of the octahedron until the exposed wires are covered. Less than 50 mg of powder are usually sufficient to surround the exposed wire. To ensure tight packing of the MgO powder, use a drill blank to tamp down the loose powder.
    4. Load a graphite capsule with the previously prepared sample material and place into the octahedron from the open side. Insert the alumina plug to complete assembly of the octahedron.
    5. On 4 of the WC cubes (**Table 2**) use polyvinyl acetate to glue short lengths of balsa-wood, one on each of the 3 faces adjacent to the truncated corner of the cube. Each balsa-wood piece should measure ~4.4 mm in height and width by ~9.0 mm in length, for the octahedron size shown in **Figure 4**. On each face, position the balsa-wood pieces in the quadrant opposite the truncated edge.
    6. Assemble 4 of the cubes to form a square in plane view, 2 with and 2 without wooden pieces attached. Orient the truncated edges to face the center of the square.
    7. Position the octahedron in the center of the cubes, so that it is supported by the truncated edges. Then angle the thermocouple arms so that they emerge from opposite corners of the square (**Figure 5A**)
    8. Place the remaining WC cubes into position to form a cube with the octahedron at its center, ensuring that the cubes with wooden pieces attached rest atop cubes that have no wooden spacers.
    9. Glue square pieces of ~0.5 mm thick G10 sheet (see Table 2) to each face of the assembled cube using a cyanoacrylate-type adhesive. For 32 mm WC cubes, use G10 sheets measuring ~55 mm x 55 mm. Two of the WC cubes have truncations that contact the resistance heater and thus form part of the electrical heating circuit. For sheets which contact these cubes, cut 2 narrow (<1 mm width) slits as indicated in **Figure 5B** and place a piece of copper foil so that it provides a point of contact between the 1st and 2nd-stage anvils.
        Note: The multi-anvil apparatus utilizes a 2-stage system of anvils contained within a retaining ring. The first stage anvils comprise 6 removable wedges that form a central cubic cavity. This cavity accommodates 8 tungsten carbide cubes with truncated corners (second stage anvils) that surround the ceramic octahedron[40]. Vertically oriented force applied to the first stage anvils by a hydraulic press is therefore transferred to the octahedron in a manner that results in quasi-hydrostatic compression of the sample. The relationship between oil pressure in the ram and sample pressure can be calibrated for the 18 mm OEL cast octahedral assembly described here using the procedures outlined by[41].
    10. Cut 2 sheets of 0.076 mm thick Mylar to the dimensions shown in **Figure 6** and coat them using a dry PTFE lubricant.
        1. Position one of the pre-cut sheets into the retaining ring (straight edge at the base) and insert the lower-set of 1st-stage anvils, which themselves are backed with 0.076 mm thick Mylar and coated with PTFE lubricant (**Figure 5B**). The lower set of anvils may be left in place between runs. Place the assembled cube into the lower set of 1st-stage anvils and connect the thermocouple arms to balanced thermocouple wires that exit the pressure module.
        2. Position the 2nd pre-cut Mylar sheet into the retaining ring (straight edge to the top) and insert the upper set of 1st-stage anvils, which should be Mylar backed and lubricated in the same manner as the lower set. This arrangement yields a lubricated Mylar to Mylar contact between the 1st-stage anvils and the retaining ring that reduces the loss of ram thrust to friction by ~30% compared to a single Mylar sheet arrangement[37].
            Note: Thicknesses and dimensions of the Mylar sheet will depend upon the exact design of the pressure module being used. Described above and in **Figure 6** are the dimensions in use at the Geophysical Laboratory, Carnegie Institution of Washington.

4. Running the Experiment

1. Once the sample is brought to the required pressure, heat at a rate of 100 K/min until the desired dwell temperature is reached. During the heating step, oil in the sample ram may need to be adjusted in order to maintain a constant oil pressure.
2. After the dwell period, quench the sample by cutting power to the furnace. Once the apparatus has cooled to RT, slowly decompress the sample.

5. Run-product Analysis

1. For piston cylinder experiments, extract the finished experiment from the pressure vessel using a hydraulic ram. With a pair of heavy-duty cutters remove the outer portions of the assembly to release the graphite capsule (piston cylinder) or furnace containing the sample capsule and support pieces (multi-anvil).
2. Mount the sample in epoxy (typically to form a 25.4 mm diameter puck) (**Figure 7A**). Using 320 to 600 grit silicon-carbide paper, grind into the sample to expose the quenched silicate melt and metallic phases. Polish the exposed surface using either alumina or diamond suspension with decreasing grit sizes ranging from ~15 to 0.3 µm.

3. Carbon coat the surface of the polished sample[42] and analyze the major element composition of the metal and silicate run-products by electron probe micro analysis (EPMA). Use a defocused (10 µm) beam diameter for the silicate analysis to avoid migration of alkali elements away from the electron beam. The analytical conditions and standards used to characterize previous samples generated with the above protocol can be found in references[29–31,35]
   Note: For experiments to investigate MSE and SSE partitioning, EPMA may also prove suitable for analysis of the tracer elements, providing they are present at sufficient concentrations.
4. Following major element analysis, remove the carbon coat using 0.3 µm alumina grit. Use laser ablation inductively coupled plasma mass spectrometry (LA-ICPMS) to determine the trace element content of the run-products. For an introduction to sample analysis by LA-ICPMS, please see reference[43].
   Note: For previous HSE solubility studies isotopes of calcium and nickel have been successfully used as internal standards to reduce the data, using both glass and sulphide reference materials respectively[29,30]. All analyses should be preceded by a single pass of ablation, followed by flushing the ablation cell for at least 60 sec. This ensures any surface contamination that may arise from polishing the experimental run-products does not affect the results.

Representative Results

The following examples and discussion focus on experiments to determine HSE solubility in silicate melts at low fO_2. For comprehensive examples of how MSE and SSE partitioning data from multi-anvil experiments may be used to constrain the *P*-*T*-fO_2 conditions of core metal segregation, the reader is referred to references[9–11]. **Figure 7B-D** displays back scattered electron images from typical experimental run-products. In experiments containing Au, the wetting properties between silicate melt, Au melt and solid HSE (Re, Os, Ir, Ru) dictate the sample geometry and result in physical separation between the silicate melt and the solid HSE. For experiments to investigate Pt, the PtIr alloy remains in direct contact with the silicate melt. Cutting power to the furnace at the end of the experiment ensures rapid cooling of the sample and quenching of the silicate melt. Run-products therefore comprise either 1 or 2 alloy phases (HSE-rich ± Au-rich) or silicate glass (providing the basalt composition of **Table 1** is used).

Contamination of the silicate glass in low fO_2 HSE solubility experiments is most readily identified by the presence of heterogeneity in time resolved LA-ICPMS spectra. This heterogeneity manifests as 'peaks' and 'troughs' in the spectra that result from the ablation of varying proportions of inclusion-bearing versus inclusion-free glass[17]. **Figure 8A** displays the time-resolved spectrum for a Pt solubility experiment that did not employ methods to prevent the formation of metal inclusions. For comparison, **Figures 8B-F** display time-resolved spectra typical for silicate run-products synthesized using the techniques outlined in the above protocol. The homogeneity of spectra b-f indicates the absence of dispersed HSE inclusions in the silicate portion of experimental run-products. Inspection of the silicate glass by scanning electron microscopy confirms the absence of visible metal-inclusions in the silicate run-products, further supporting a lack of contamination. The spectra displayed in **Figure 8A-E** are from run-products synthesized as part of several previous studies[29–31]. **Figure 8F** is from a Ru solubility experiment performed at 2,273 K and 2 GPa using the Au-addition technique described above. The homogeneity of this spectra suggests that this approach is also successful in avoiding the formation of metal-inclusions found in previous Ru solubility experiments performed at similarly reducing conditions (~IW+2.5)[24].

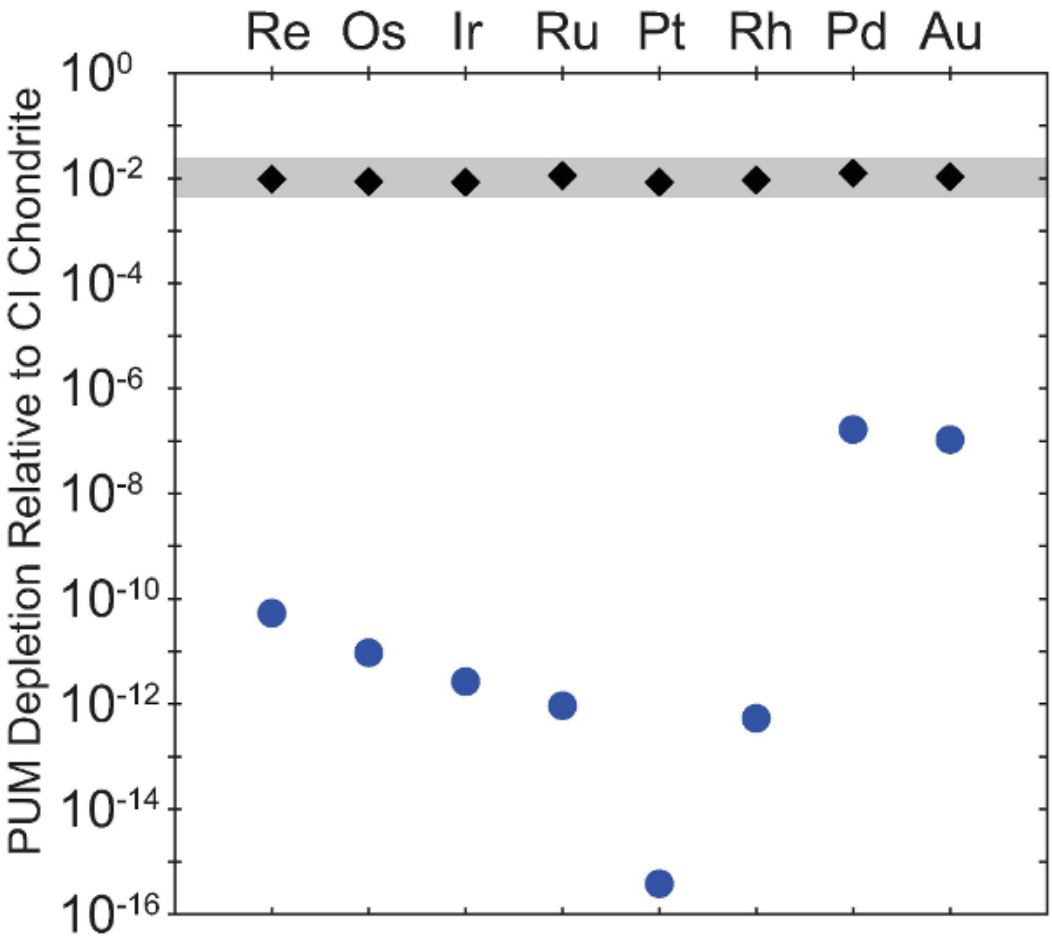

Figure 1. Comparison between the estimated primitive upper mantle (PUM) composition and that predicted by the results of solubility experiments at low pressure and temperature. Data for the PUM composition from Fischer-Gödde *et al.*[7]. Partition coefficients for the HSE are at 0.1 MPa, 1573-1673 K and IW-2 from Fe-free experiments by [27](Re), [44](Os), [18](Ir), [45](Ru), [16](Pd), [46](Au), [21](Pt and Rh). Please click here to view a larger version of this figure.

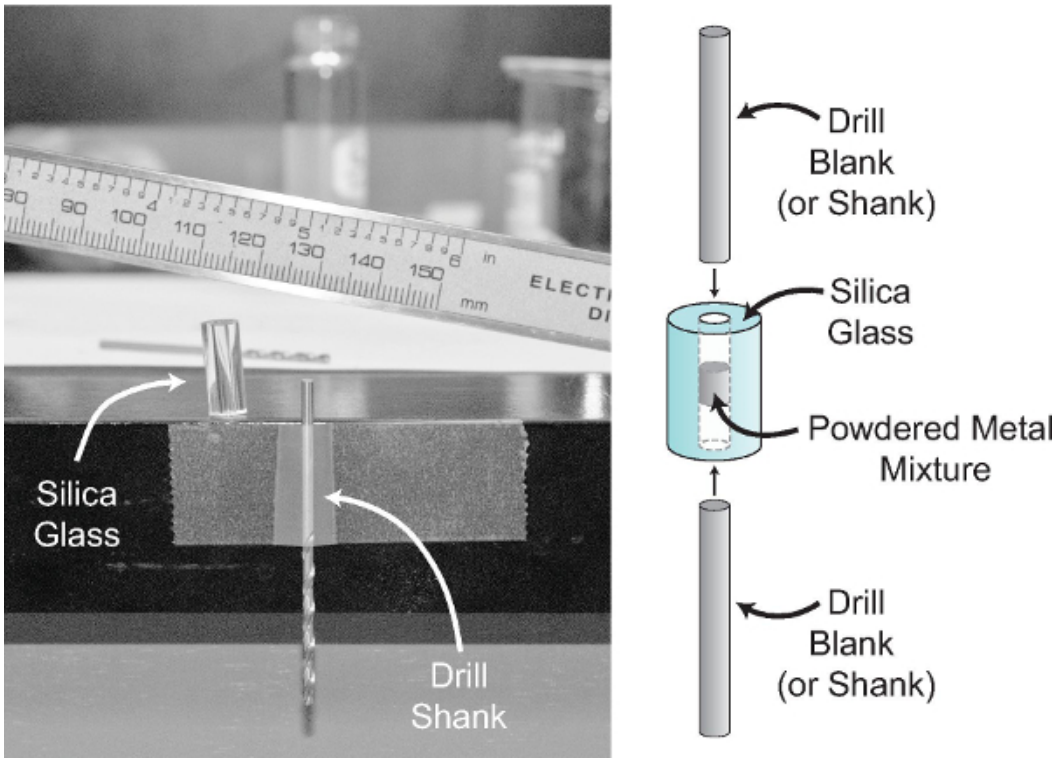

Figure 2. Arrangement used to cold-press metallic powders. The lower drill blank (or shank) is initially taped to the edge of a workbench to allow easy loading of the powders into the silica glass tube. Please click here to view a larger version of this figure.

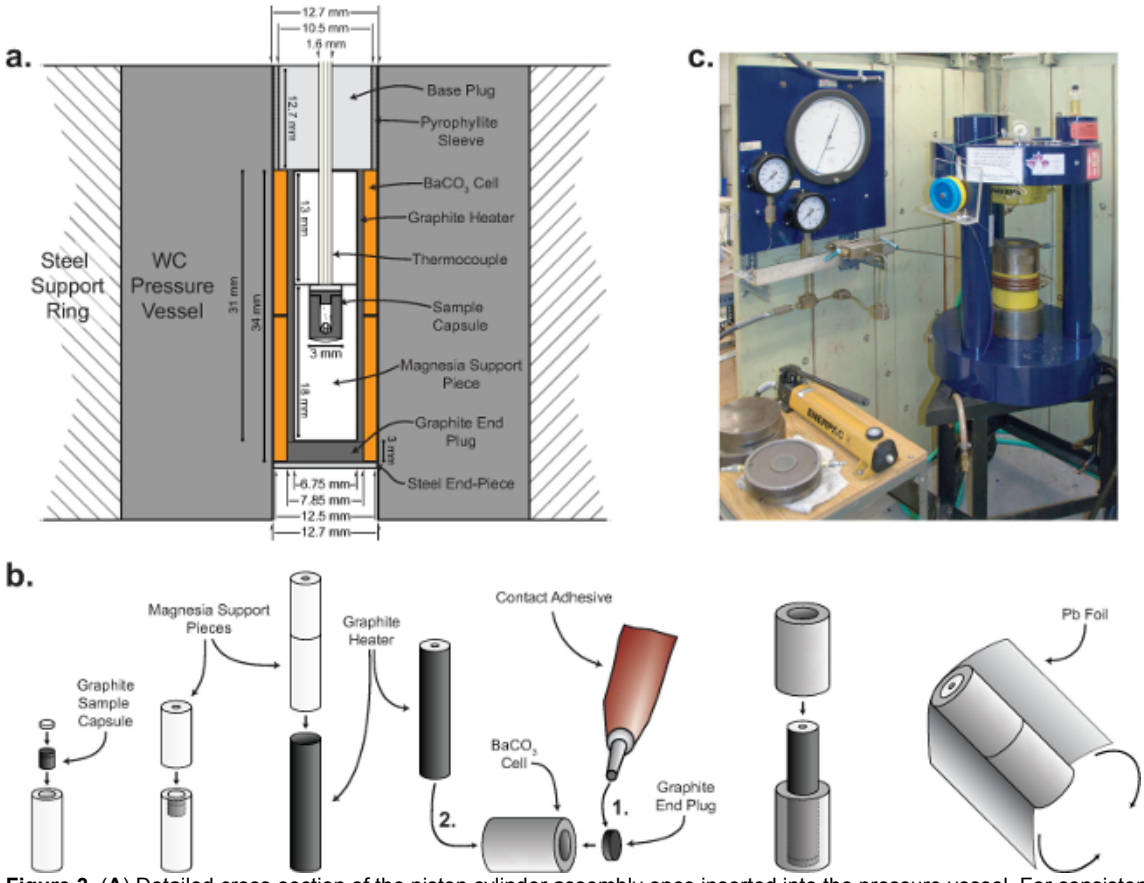

Figure 3. (**A**) Detailed cross-section of the piston cylinder assembly once inserted into the pressure vessel. For consistent results, the clearance between components within the resistance furnace should be within 0.025 mm of the nominal values[38]. $BaCO_3$ cells should be within ~0.13 mm of the nominal inner and outer diameters. Details for the construction of a suitable die may be found in [47], although the cell inner diameter should be modified from the drawings in this reference to 7.9 mm. (**B**) Procedure for constructing the piston cylinder sample assembly. Either a cyanoacrylate glue or household cement are suitable to secure the graphite end plug in the $BaCO_3$ sleeve, however, no more than ~10 mg should be applied. (**C**) A piston cylinder press at the University of Toronto. Please click here to view a larger version of this figure.

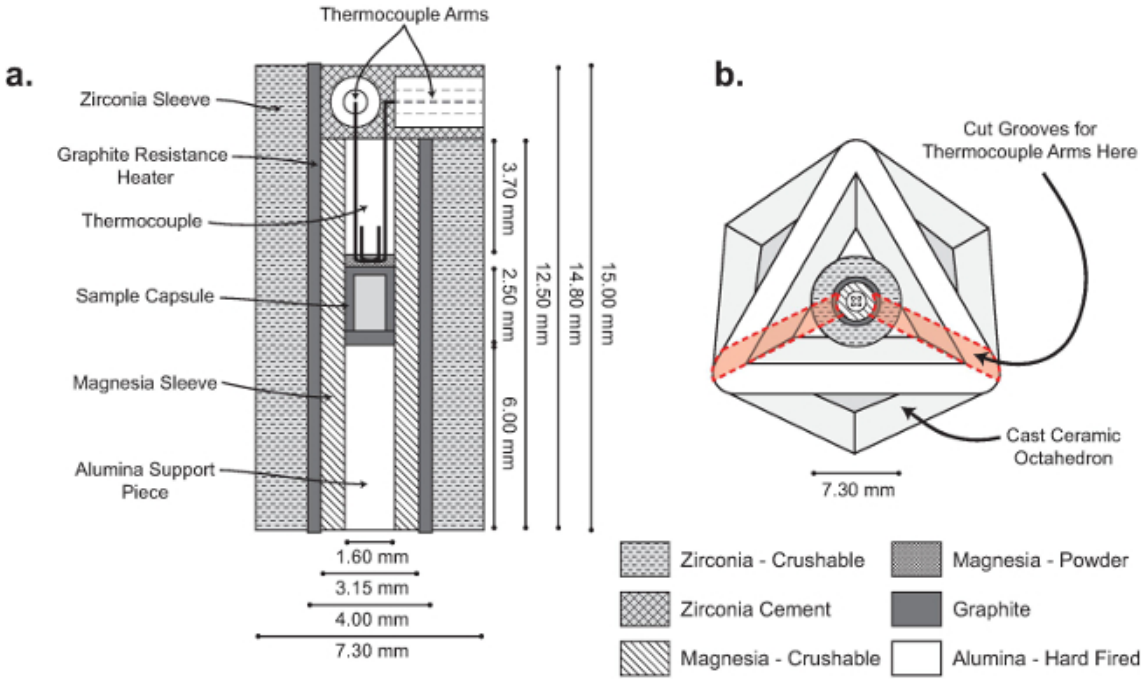

Figure 4. (**A**) Cross-section of multi-anvil assembly suitable for use with WC cubes that have an 11 mm TEL. The uppermost part of the figure is drawn to show how the thermocouple arms exit the octahedron, as viewed both perpendicular-to and down the axis of the wire as indicated. (**B**) Top view of cast octahedron with gasket fins. Grooves for the thermocouple arms should be cut into the areas marked in red. Note that the inner magnesia sleeve and 4-hole alumina tube shown in the figure should not be in place when the grooves are cut. Please click here to view a larger version of this figure.

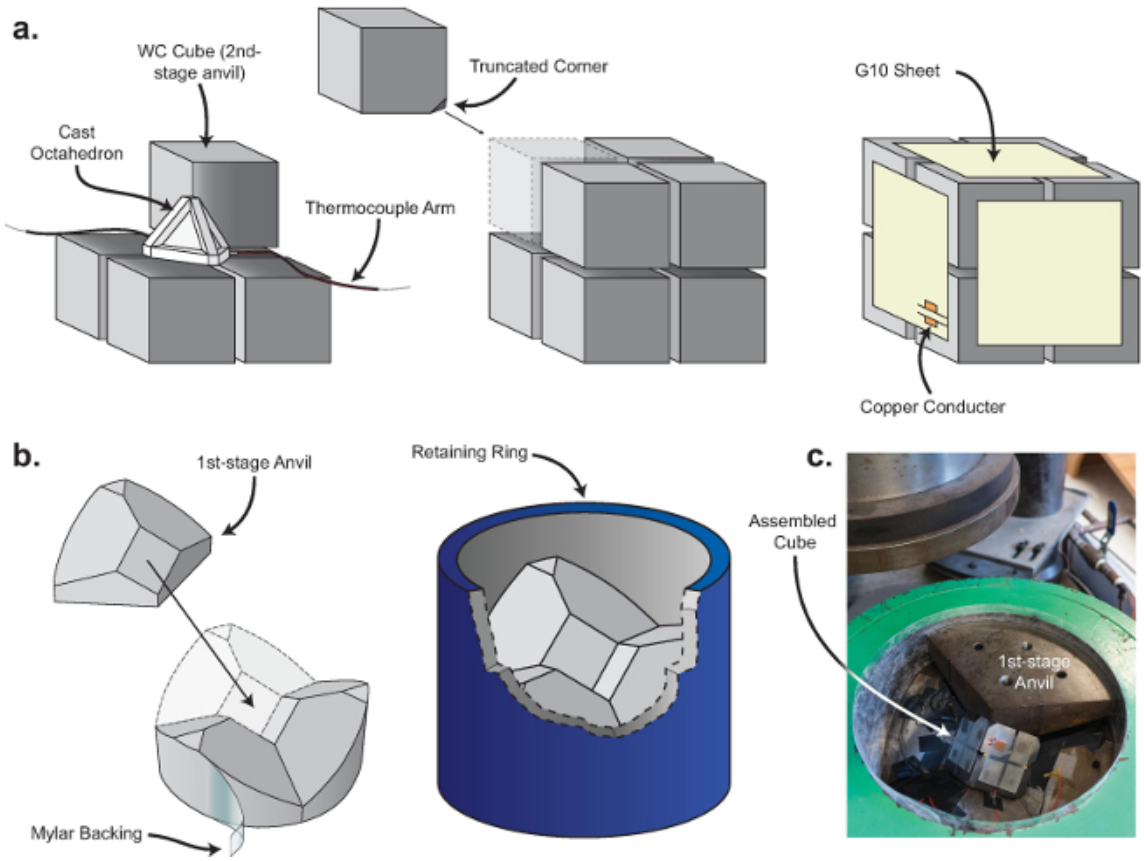

Figure 5. (**A**) Arrangement of the WC cubes around the assembled octahedron. (**B**) Lower set of 1st-stage anvils and their arrangement within the retaining ring. (**C**) Completed experiment placed into the pressure module with 1 of the upper set of 1st-stage anvils in place. Please click here to view a larger version of this figure.

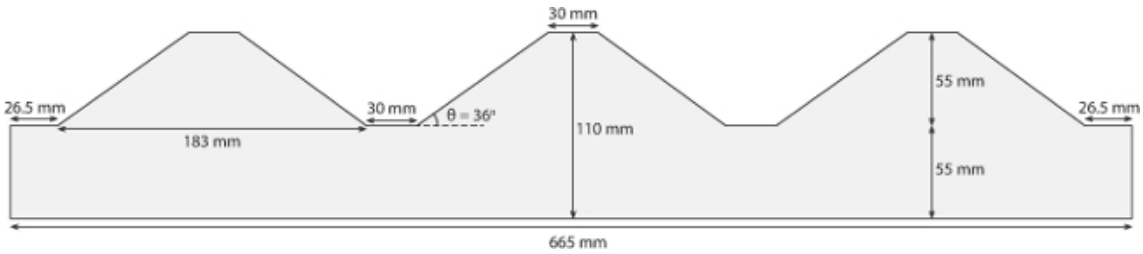

Figure 6. Dimensions of the mylar sheet described in step 3.2.10. Please click here to view a larger version of this figure.

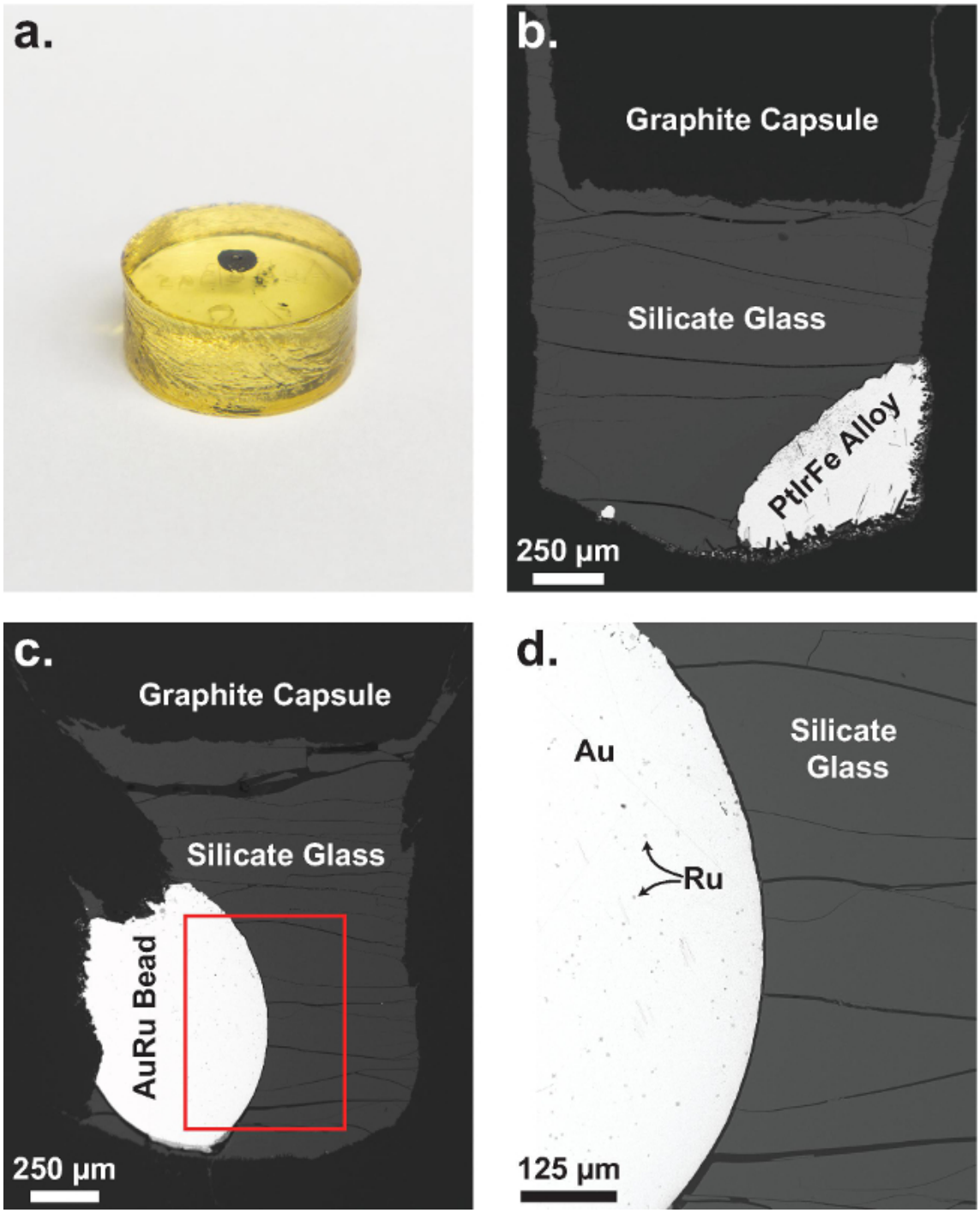

Figure 7. (**A**) Experimental run-product mounted in epoxy, then ground and polished. (**B**) and (**C**) Back-scattered electron images of experimental run-products from experiments using the Si-addition (**B**) and Au-addition (**C**) techniques described in the text for experiments to determine Pt and Ru solubility respectively. Image (**B**) is reprinted from [31] with permission from Elsevier. (**D**) Enlarged view of the area outlined in red on (**C**) to show the detail of the AuRu bead and metal-silicate interface. Please click here to view a larger version of this figure.

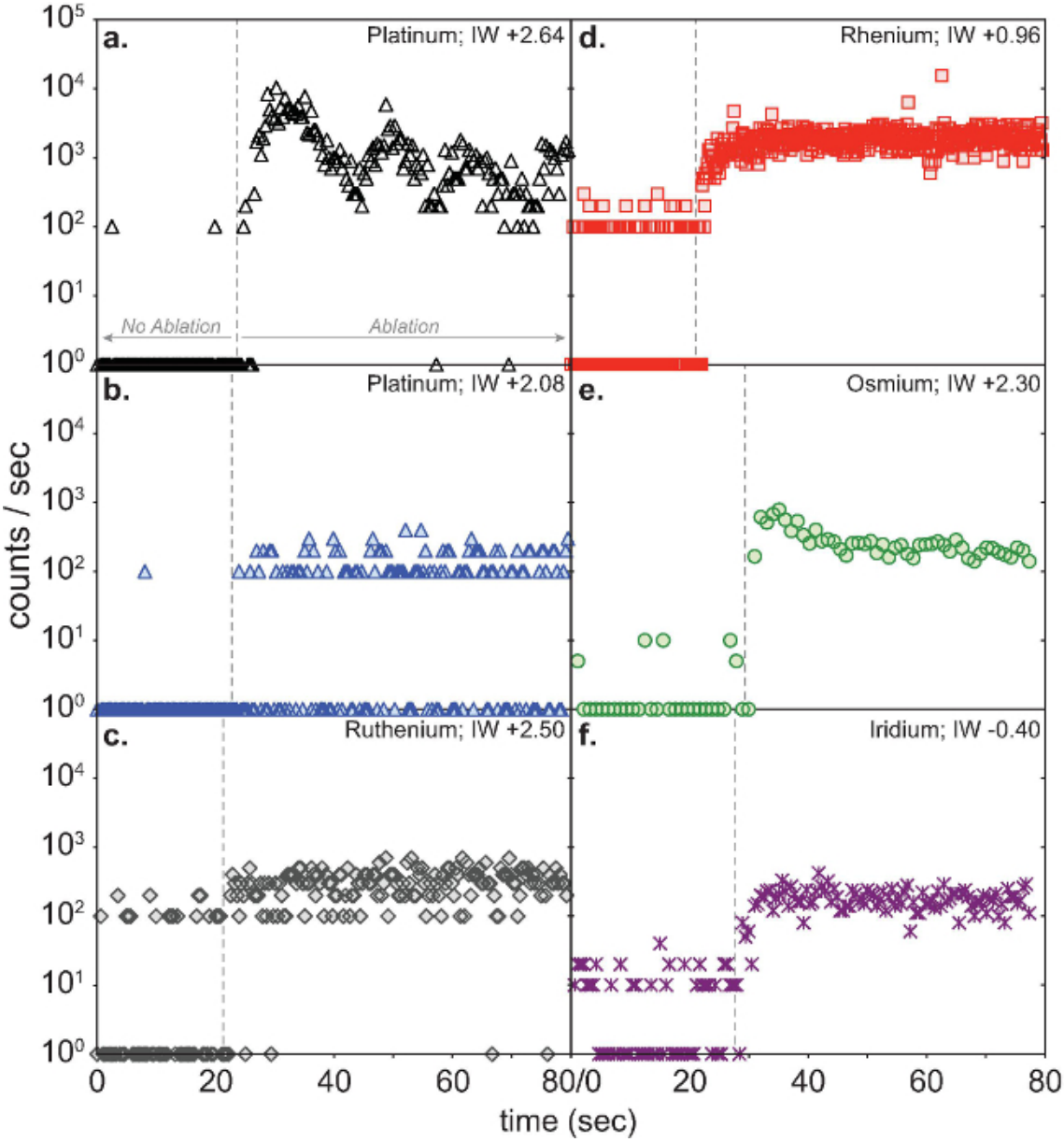

Figure 8. (**A**) Time-resolved LA-ICP-MS spectra from a low fO_2 Pt-solubility experiment that did not employ measures to suppress the formation of metal inclusions. (**B-F**) Typical time-resolved LA-ICP-MS spectra from experiments for Ru, Pt[31], Re[30], Os and Ir[29] that were performed using the procedure outlined in the text. All data shown are from experiments performed at 2,273 K and 2 GPa. The vertical dashed line in each figure separates the region of ablation from the region of background acquisition. Please click here to view a larger version of this figure.

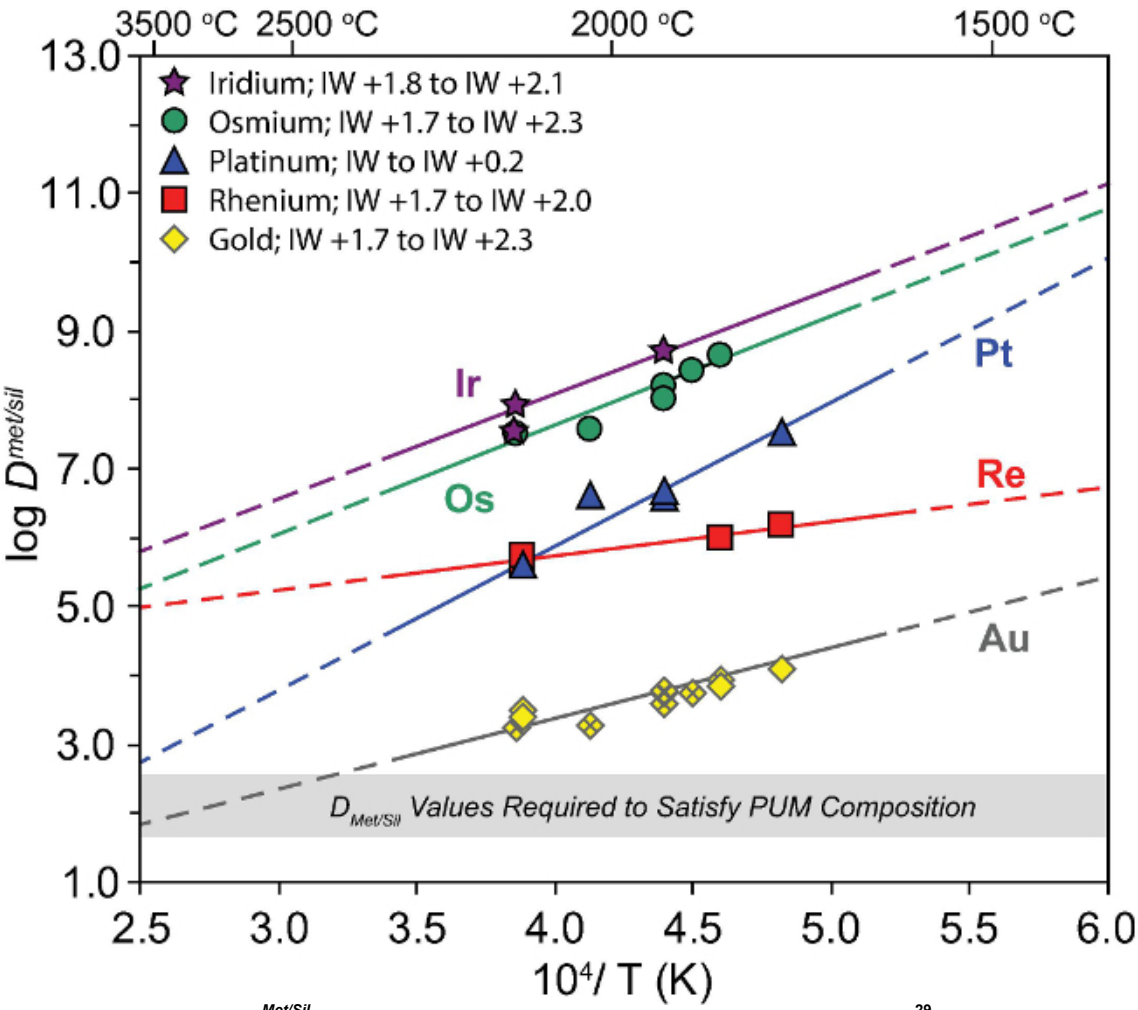

Figure 9. The change in $D^{Met/Sil}$ with *T* for experiments performed by Brenan & McDonough[29] (Os, Ir, Au), Bennett & Brenan[30] (Re, Au) and Bennett *et al.*[31] (Pt) using the procedures described here. All data are from experiments done at 2 GPa. Please click here to view a larger version of this figure.

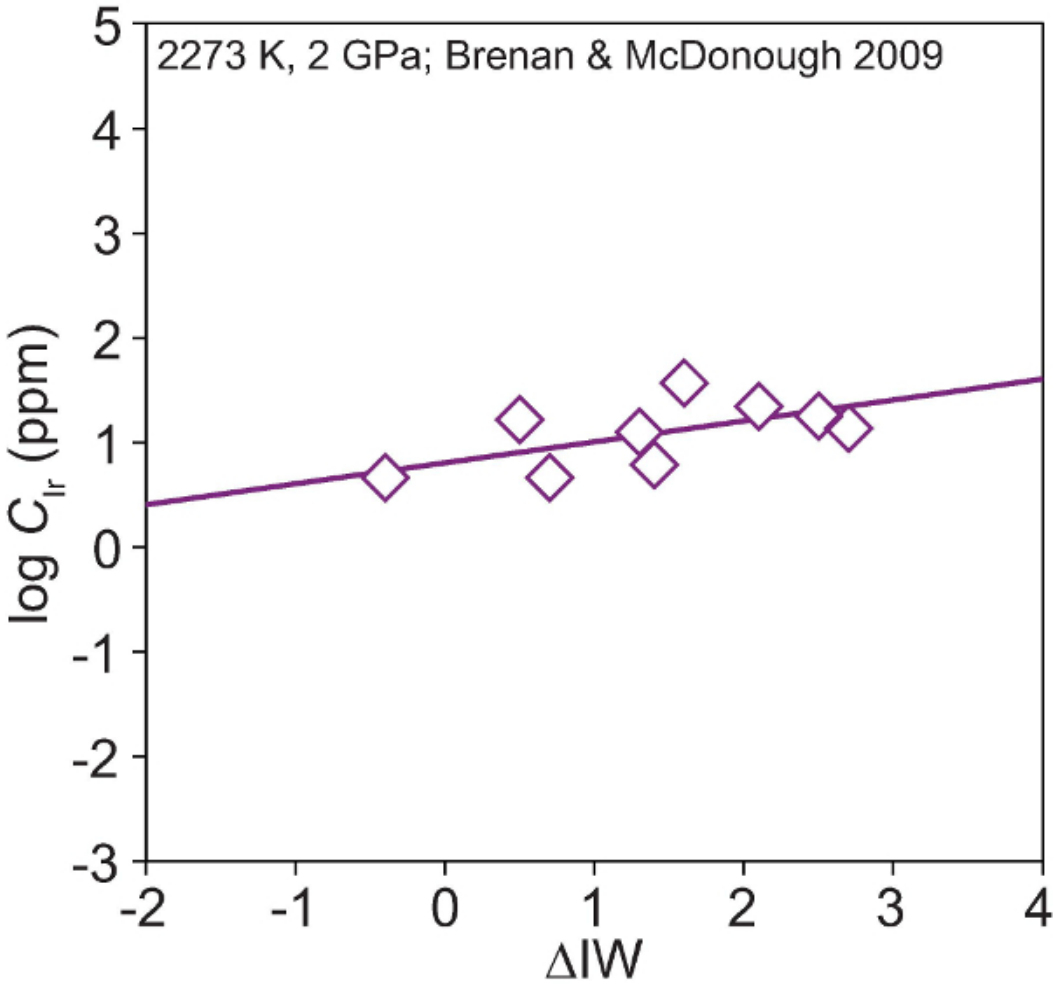

Figure 10. The solubility of Iridium in basaltic melt at 2,273 K and 2 GPa as a function of fO_2 relative to the iron-wüstite (IW) buffer. Data are from Brenan & McDonough[29]. Please click here to view a larger version of this figure.

	Before Decarbonation			After Decarbonation	
	wt% Oxides/ Carbonates; Fe^{2+} Starting Composition	**wt% Oxides/ Carbonates; Fe^{2+} Starting Composition**		**wt% Oxide; Fe^{2+} Starting Composition**	**wt % Oxide; Fe^{3+} Starting Composition**
SiO_2	47.92	47.40	SiO_2	51.87	51.26
Al_2O_3	9.91	9.80	Al_2O_3	10.73	10.60
$CaCO_3$	16.20	16.02	CaO	9.83	9.71
MgO	14.58	14.42	MgO	15.79	15.60
FeO	9.84	-	FeO	10.66	-
Fe_2O_3	-	10.82	Fe_2O_3	-	11.71
MnO	0.06	0.06	MnO	0.07	0.07
Na_2CO_3	1.20	1.19	Na_2O	0.76	0.75
NiO	0.28	0.27	NiO	0.30	0.30

Table 1.

Discussion

The results of inclusion-free experiments performed using the protocols outlined here have previously been compared with literature data in references[29] (Os, Ir, Au), [30] (Re, Au) and [31] (Pt). Pt is most instructive in demonstrating the usefulness of inclusion-free run-products. For experiments run at low fO_2, Ertel *et al.*[48] assigned inclusions to a stable origin and therefore restricted data reduction to the lowest counts-

per-second region of time-resolved LA-ICPMS spectra. This approach minimizes the contribution of inclusions to the measured silicate melt concentrations. Data from Ertel *et al.*[48] at ~IW+1 agree well with the trend between $D^{Met/Sil}$ and $1/T$ defined by inclusion-free experiments performed at similar fO_2; confirming that their chosen analytical treatment is effective in determining true Pt solubilities[31]. Furthermore, experiments done using the inclusion-suppressing protocol outlined here are able to probe more reducing conditions, in which the spectrum filtering method becomes less effective[17]. In studies that assume only the presence of quench related inclusions, there is variable agreement with the inclusion-free data. For example, good agreement is observed with the results of Mann *et al.*[49], however, the experiments of Cottrell *et al.*[22] display systematically lower values of $D^{Met/Sil}$ than inclusion-free experiments[31]. The generation of inclusion-free experiments at a wide range of conditions is thus crucial to assess the reliability of previous inclusion-contaminated measurements.

Although the protocol described here has proven successful over a range of conditions, it is not a panacea for the problem of contamination by metal inclusions. Experiments performed using the technique of Au addition are affected by the formation of complex alloy compositions at very low fO_2. In order to generate conditions significantly more reducing than the iron-wüstite buffer, elemental Si is added to the starting materials. Run products from the most reducing of these experiments contain 2 co-existing alloys which possess extensive quench related exsolution textures. Immiscibility in the alloy appears to arise due to the significant solution of Si into the metal phase at reducing conditions. A lack of suitable activity-composition data for the alloy compositions formed at very reducing conditions prevents the Fe and HSE activities in the alloy phase from being determined. This prevents accurate calculation of sample fO_2 and HSE concentrations in the silicate melt at the solubility limit.

The efficacy of Si-addition as a method to prevent formation of Pt inclusions appears to decrease at lower temperatures. Bennett *et al.*[31] noted that experiments performed at 1,873 K display evidence for contamination by metal inclusions, whereas those done at higher temperatures do not. This may be due to a change in the kinetic relationship between sample reduction and Pt in-diffusion at lower temperatures. A further consideration for experiments performed using the Si-addition technique is it's effect on the final melt composition. Oxidation of elemental Si early in the experiment occurs *via* the following reaction with FeO in the melt:

$$Si(met) + 2FeO(sil) = SiO_2(sil) + 2Fe(met) \quad (2)$$

Addition of greater quantities of Si, in order to access more reducing conditions, therefore results in a more SiO_2 enriched and FeO depleted melt composition. In order to conduct experiments that span a wide fO_2 range, but have little variation in melt composition, suitable adjustment of the silicate starting material should be made in order to compensate for reaction 6. Broadly, this can be accomplished by adding 2 moles of FeO and removing 1 mole of SiO_2 for each mole of Si added to the starting composition. It should also be noted that some studies have found the occurrence of metallic inclusions also depends upon melt composition, in particular whether the melt is Fe-bearing[50].

The solubility data afforded by uncontaminated run-products allows accurate metal-silicate partition coefficients to be calculated. For experiments in which the HSE of interest is not present as a pure phase (*i.e.,* HSE metal activity <1), concentrations measured in the silicate phase are corrected to unit activity using available thermodynamic data. With the exception of Au, a useful summary of the available activity-composition relations for HSE alloys is provided in reference[49]. Limited data for Au-Fe alloys may be found in references[46,51]. The following relation is then used to determine values of $D^{Met/Sil}$ from the corrected HSE concentrations in silicate melt[16]

$$D_{HSE}^{Met/Sil} = \frac{1}{C_{HSE}^{SilSat} \times A \times \gamma_{HSE}^{Fe\infty}} \quad (3)$$

Where C_{HSE}^{SilSat} is the HSE concentration of the silicate at saturation in the HSE phase, A is a mole to weight conversion factor and $\gamma_{HSE}^{Fe\infty}$ is the activity coefficient of the chosen HSE at infinite dilution in liquid Fe-metal. **Figure 9** displays the change in $D^{Met/Sil}$ with T calculated from experiments done at 2 GPa and an fO_2 close to the iron-wüstite buffer. One application of this data is to assess the ability of high temperature metal-silicate equilibrium to account for the estimated primitive upper mantle abundance of these elements. Values of $D^{Met/Sil}$ for the HSE must decrease to values of ~10^2–10^3 at approximately the same temperature if metal-silicate equilibrium is responsible for the PUM composition. The data from previous studies displayed in **Figure 9** suggests this requirement is not met by the results of experiments performed at reducing conditions[29–31].

Solubility measurements from uncontaminated silicate run-products are also useful in revealing the speciation of HSEs dissolved in silicate melt at low fO_2. Information regarding the speciation of these metals over a large range of redox conditions is useful not only for guiding extrapolation of the data beyond the experimentally studied range, but also for the informed design of glasses with particular optical properties. Changes in the oxidation state of dissolved metals may be accompanied by changes in their co-ordination chemistry, from which variation in properties such as optical absorbance may arise. For example the dissolution of platinum, widely used as a container material for synthesizing glass from melt, may lead to different colored glasses depending upon the redox conditions of the melt[52,53]. The oxidation state of dissolved HSEs can be inferred from the change in solubility with fO_2. Consider dissolution of a metal (M) as an oxide species in the melt:

$$M(met) + \frac{n}{4}O_2(g) = M^{n+}O_{n/2}(sil) \quad (4)$$

Where n is the oxidation state of the dissolved metal. The equilibrium constant (K) at P and T for equation 3 is given by:

$$K_{P,T} = \left[\frac{a_{MO_{n/2}}}{(a_M)(fO_2)^{\frac{n}{4}}} \right]_{P,T} \quad (5)$$

Equating ln$K$ with the Gibbs free energy of reaction, and at saturation in the metal phase (a_M = 1), equation 4 becomes:

$$\ln X_{MO_{n/2}} = \frac{n}{4}\ln fO_2 - \ln \gamma_{MO_{n/2}} - \frac{\Delta G^{o}_{P,T}}{RT} = \frac{n}{4}\ln fO_2 + constant \quad (6)$$

The slope of a trend between HSE solubility and fO_2 therefore yields n/4, from which the speciation may be obtained. Brenan & McDonough[29] determined the solubility of Ir as a function of fO_2 from experiments which used the techniques described here. The results of these experiments are displayed in **Figure 10** and yield a slope of 0.2, largely consistent with a 1+ oxidation state (predicted slope of 0.25) for Ir in reduced silicate melts.

Experimentally determined metal-silicate partition coefficients can be used to establish the conditions of core-mantle equilibrium during terrestrial accretion. Results for the highly siderophile elements can also be used to assess whether the Earth experienced a late-veneer of chondritic material subsequent to core formation. Outlined here are procedures to perform metal-silicate partitioning and solubility experiments in the multi-anvil and piston-cylinder devices respectively. Techniques are also described that suppress the formation of metal inclusions in HSE solubility experiments at 2 GPa and temperatures >1,873 K. The calculated HSE partition coefficients suggest that metal-silicate equilibrium at high T does not explain the apparent excess of HSEs in primitive upper mantle. Future work remains to confirm if the HSE partitioning behavior indicated by experiments at 2 GPa persists to higher P and T. This will require testing the inclusion-suppressing protocols outlined here in a high P multi-anvil experimental design.

Disclosures

The Authors have nothing to disclose.

Acknowledgements

This work was supported by the Natural Sciences and Engineering Research Council of Canada Equipment, Discovery and Discovery Accelerator Grants awarded to J.M.B. N.R.B acknowledges support from the Carnegie Institution of Washington post-doctoral fellowship program. Stephen Elardo is also thanked for his assistance prior to filming with the piston-cylinder press at the Geophysical Lab.

References

1. Canup, R. M. Dynamics of Lunar Formation. *Annual Review of Astronomy and Astrophysics.* **42**, 441-475 (2004).
2. Rubie, D., Nimmo, F., Melosh, H. Formation of Earth's core. *Treatise on geophysics.* **9**, 51-90 (2007).
3. Karato, S., Murthy, V. R. Core formation and chemical equilibrium in the Earth Physical considerations. *Physics of the Earth and Planetary Interiors.* **100**, 61-79 (1997).
4. Dziewonski, A. M., Anderson, D. L. Preliminary reference Earth model. *Physics of the Earth and Planetary Interiors.* **25**, (4), 297-356 (1981).
5. McDonough, W., Sun, S. The composition of the Earth. *Chemical geology.* **120**, (3-4), 223-253 (1995).
6. Palme, H., O'Neill, H. Cosmochemical estimates of mantle composition. *Treatise on geochemistry.* **2**, 1-38 (2003).
7. Fischer-Gödde, M., Becker, H., Wombacher, F. Rhodium, gold and other highly siderophile elements in orogenic peridotites and peridotite xenoliths. *Chemical Geology.* **280**, (3-4), 365-383 (2011).
8. Ringwood, A. E. Chemical evolution of the terrestrial planets. *Geochimica et Cosmochimica Acta.* **30**, 41-104 (1966).
9. Wood, B. J., Wade, J. Core formation and the oxidation state of the Earth. *Earth and Planetary Science Letters.* **236**, (1-2), 78-95 (2005).
10. Siebert, J., Corgne, A., Ryerson, F. Systematics of metal–silicate partitioning for many siderophile elements applied to Earth's core formation. *Geochimica et Cosmochimica Acta.* **75**, (6), 1451-1489 (2011).
11. Righter, K. Prediction of metal–silicate partition coefficients for siderophile elements: an update and assessment of PT conditions for metal–silicate equilibrium during accretion of. *Earth and Planetary Science Letters.* **304**, (1-2), 158-167 (2011).
12. Wood, B. J., Walter, M. J., Wade, J. Accretion of the Earth and segregation of its core. *Nature.* **441**, (7095), 825-833 (2006).
13. Kimura, K. A. N., Lewis, R. O. Y. S., Anders, E. Distribution of gold and rhenium between nickel-iron and silicate melts: implications for the abundance of siderophile elements on the Earth and Moon. *Geochimica et Cosmochimica Acta.* **38**, 683-701 (1974).
14. Murthy, V. R. Early differentiation of the Earth and the problem of mantle siderophile elements: a new approach. *Science.* **253**, (5017), 303-306 (1991).
15. Righter, K., Humayun, M., Danielson, L. Partitioning of palladium at high pressures and temperatures during core formation. *Nature Geoscience.* **1**, (5), 321-323 (2008).
16. Borisov, A., Palme, H., Spettel, B. Solubility of palladium in silicate melts Implications for core formation in the Earth. *Geochimica et Cosmochimica Acta.* **58**, (2), 705-716 (1994).
17. Ertel, W., Dingwell, D. B., Sylvester, P. J. Siderophile elements in silicate melts — A review of the mechanically assisted equilibration technique and the nanonugget issue. *Chemical Geology.* **248**, (3-4), 119-139 (2008).
18. Borisov, A. L., Palme, H. The solubility of iridium in silicate melts: New data from experiments with Ir10Pt90 alloys. *Geochimica et Cosmochimica Acta.* **59**, (3), 481-485 (1995).
19. Borisov, A., Palme, H. Experimental determination of Os metal/silicate partitioning. *Neues Jahrbuch für Mineralogie - Abhandlungen.* **172**, (2-3), 347-356 (1998).
20. Borisov, A., Palme, H. Experimental determination of the solubility of platinum in silicate melts. *Geochimica et Cosmochimica Acta.* **61**, (20), 4349-4357 (1997).
21. Ertel, W., O'Neill, H. S. C., Sylvester, P. J., Dingwell, D. B. Solubilities of Pt and Rh in a haplobasaltic silicate melt at 1300. *C. Geochimica et Cosmochimica Acta.* **63**, (16), 2439-2449 (1999).
22. Cottrell, E., Walker, D. Constraints on core formation from Pt partitioning in mafic silicate liquids at high temperatures. *Geochimica et Cosmochimica Acta.* **70**, (6), 1565-1580 (2006).

23. Yokoyama, T., Walker, D., Walker, R. J. Low osmium solubility in silicate at high pressures and temperatures. *Earth and Planetary Science Letters.* **279**, (3-4), 165-173 (2009).
24. Laurenz, V., Fonseca, O. C., Ballhaus, C., Peter, K., Heuser, A., Sylvester, P. J. The solubility of palladium and ruthenium in picritic melts: 2. The effect of sulfur. *Geochimica et Cosmochimica Acta.* **102**, 172-183 (2013).
25. Neill, H. S. C. Experimental petrochemisty of some highly siderophile elements at high temperatures, and some implications for core formation and the mantle's early history. *Chemical Geology.* **120**, (3-4), 255-273 (1995).
26. Fortenfant, S. S., Dingwell, D. B., Ertel-Ingrisch, W., Capmas, F., Birck, J. L., Dalpé, C. Oxygen fugacity dependence of Os solubility in haplobasaltic melt. *Geochimica et Cosmochimica Acta.* **70**, (3), 742-756 (2006).
27. Ertel, W., O'Neill, H. S. C., Sylvester, P. J., Dingwell, D. B., Spettel, B. The solubility of rhenium in silicate melts: Implications for the geochemical properties of rhenium at high temperatures. *Geochimica et Cosmochimica Acta.* **65**, (13), 2161-2170 (2001).
28. Medard, E., Schmidt, M. W., Wahle, M., Keller, N. S., Gunther, D. Pt in Silicate Melts: Centrifuging Nanonuggets to Decipher Core Formation Processes. *Lunar and Planetary Science Conference.* 3-4 (2010).
29. Brenan, J., McDonough, W. Core formation and metal–silicate fractionation of osmium and iridium from gold. *Nature Geoscience.* **2**, (11), 798-801 (2009).
30. Bennett, N. R., Brenan, J. M. Controls on the solubility of rhenium in silicate melt: Implications for the osmium isotopic composition of Earth's mantle. *Earth and Planetary Science Letters.* **361**, 320-332 (2013).
31. Bennett, N., Brenan, J., Koga, K. The solubility of platinum in silicate melt under reducing conditions: Results from experiments without metal inclusions. *Geochimica et Cosmochimica Acta.* **133**, 422-442 (2014).
32. Okamoto, H., Massalski, T. B. The Au-Pt (Gold-Platinum) System. *Bulletin of Alloy Phase Diagrams.* **6**, (1), 46-55 (1985).
33. Neill, H., Pownceby, M. Thermodynamic data from redox reactions at high temperatures. I. An experimental and theoretical assessment of the electrochemical method using stabilized zirconia. *Contributions to Mineralogy and Petrology.* **114**, (3), 296-314 (1993).
34. Deines, P., Nafziger, R., Ulmer, G., Woermann, E. *Temperature-oxygen fugacity tables for selected gas mixtures in the system CHO at one atmosphere total pressure. Bulletin of the Earth and Mineral Sciences Experiment Station.* (88), Pennsylvania State University University Park, Pennsylvania (1974).
35. Corgne, A., Keshav, S., Wood, B. J., McDonough, W. F., Fei, Y. Metal–silicate partitioning and constraints on core composition and oxygen fugacity during Earth accretion. *Geochimica et Cosmochimica Acta.* **72**, (2), 574-589 (2008).
36. Agee, C. B., Walker, D. Static compression and olivine flotation in ultrabasic silicate liquid. *Journal of Geophysical Research.* **93**, (7), 3437-3449 (1988).
37. Walker, D. Lubrication, gasketing, and precision in multianvil experiments. *American Mineralogist.* **76**, (7-8), 1092-1100 (1991).
38. Boyd, F., England, J. Apparatus for Phase-Equilibrium Measurements at Pressures up to 50 Kilobars and Temperatures up to 1750. *C. Journal of Geophysical Research.* **65**, (2), 741-748 (1960).
39. McDade, P., Wood, B. J., *et al.* Pressure corrections for a selection of piston-cylinder cell assemblies. *Mineralogical Magazine.* **66**, (6), 1021-1028 (2002).
40. Walker, D., Carpenter, M., Hitch, C. Some simplifications to multianvil devices for high pressure experiments. *American Mineralogist.* **75**, (9-10), 1020-1028 (1990).
41. Bertka, C. M., Fei, Y. Mineralogy of the Martian interior up to core-mantle boundary pressures. *Journal of Geophysical Research.* **102**, (B3), 5251 (1997).
42. Reed, S. J. B. *Electron Microprobe Analysis and Scanning Electron Microscopy in Geology.* Cambridge University Press: Cambridge, UK (2005).
43. Sylvester, P. J. *Laser Ablation ICP-MS in the Earth Sciences: Current Practices and Outstanding Issues.* Mineralogical Association of Canada Quebec (2008).
44. Borisov, A., Walker, R. Os solubility in silicate melts: New efforts and results). *American Mineralogist.* **85**, (7-8), 912-917 (2000).
45. Borisov, A., Nachtweyh, K. Ru Solubility in Silicate Melts: Experimental Results in Oxidizing Region. *Lunar and Planetary Science Conference.* **77058**, 1320 (1998).
46. Borisov, A., Palme, H. Experimental determination of the solubility of Au in silicate melts. *Mineralogy and Petrology.* **56**, (3-4), 297-312 (1996).
47. Dunn, T. The Piston-Cylinder Apparatus. *Short Course Handbook on Experiments at High Pressure and Applications to the Earth's Mantle.* 39-94 (1993).
48. Ertel, W., Walter, M., Drake, M., Sylvester, P. Experimental study of platinum solubility in silicate melt to 14GPa and 2273K: implications for accretion and core formation in Earth. *Geochimica et Cosmochimica Acta.* **70**, (10), 2591-2602 (2006).
49. Mann, U., Frost, D., Rubie, D. Partitioning of Ru. Rh, Pf, Re, Ir and Pt between liquid metal and silicate at high pressures and high temperatures-Implications for the origin of highly siderophile element concentrations in the Earth's mantle. *Geochimica et Cosmochimica Acta.* **84**, 593-613 (2012).
50. Laurenz, V., Fonseca, R. O. C., Ballhaus, C., Sylvester, P. J. Solubility of palladium in picritic melts 1 . The effect of iron. *Geochimica et Cosmochimica Acta.* **74**, (10), 2989-2998 (2010).
51. Liu, Y., Ge, Y., Yu, D. Thermodynamic descriptions for Au–Fe and Na–Zn binary systems. *Journal of Alloys and Compounds.* **476**, (1-2), 79-83 (2009).
52. Rindone, G. E., Rhoads, J. L. The Colors of Platinum, Palladium, and Rhodium in Simple Glasses. *Journal of the American Ceramic Society.* **39**, (5), 173-180 (1956).
53. Akai, T., Nishii, J., Yamashita, M., Yamanaka, H. Chemical behavior of platinum-group metals in oxide glasses. *Journal of Non-Crystalline Solids.* **222**, (Special Issue), 304-309 (1997).

